Spring 2019

Detecting the cold: Do innexins function in cold nociception?

Rachel Barborek

Detecting the Cold: Do Innexins Function in Cold Nociception?

An Honors College Project Presented to

the Faculty of the Undergraduate

College of Science and Mathematics

James Madison University

by Rachel M. Barborek

April 2019

Accepted by the faculty of the Biology and Biotechnology Departments, James Madison University, in partial fulfillment of the requirements for the Honors College.

FACULTY COMMITTEE:

Project Advisor: Susan Halsell, Ph.D.
Associate Professor, Assistant Dept. Head,
Department of Biology

Reader: Corey Cleland, Ph.D.
Associate Professor, Department of Biology

Reader: Timothy Bloss, Ph.D.
Associate Professor, Department of Biology

HONORS COLLEGE APPROVAL:

Bradley R. Newcomer, Ph.D.,
Dean, Honors College

PUBLIC PRESENTATION

This work is accepted for presentation, in part or in full, at Biosymposium on April 12, 2019.

Dedication Page

I dedicate this thesis to my family: Susan, Todd, and Decker Barborek for instilling in me a passion for putting forth my best effort in all my endeavors.

Acknowledgements

I would like to thank Kendyl Combs, Althea Neighbors, and Matthew Knick for contributing 75% of the cold behavioral assay data. I thank Dr. Kristopher Kubow for his help with confocal microscopy. I would especially like to thank Dr. Susan Halsell for helping me craft this thesis, and I thank the members of my reading committee, Dr. Corey Cleland and Dr. Timothy Bloss, for helping refine it.

Table of Contents

List of Tables

List of Figures

ABSTRACT

Nociception is the perception of and response to harmful stimuli. Nociception is essential for minimizing tissue damage, but aberrant nociceptive pathways can result in chronic pain. Chronic pain in the U.S. is commonly managed with wide-acting opioids, and precisely defining the components of nociceptive pathways could uncover novel targets for pain therapies. I hypothesize that the vitally quick process of nociception would utilize electrical synapses because they transmit signals between neurons more quickly than chemical synapses do. This study, therefore, aims to uncover the potential role of the eight *Drosophila melanogaster* gap junction proteins, the Innexins, in cold nociception. Wild type *Drosophila* larvae exhibit a characteristic full-body contraction, or cringe, in response to noxious cold. The expression level of individual Innexins was knocked down in the peripheral dendritic arborization (da) neurons that mediate cold nociception via the *Drosophila* GAL4/UAS RNAi system. Knocked-down larvae were subjected to a cold behavioral assay, and their behavior was videotaped and analyzed to quantify the "percent cringe" value in order to identify the number of "non-cringers" for statistical analysis. By comparing the proportion of non-cringers between the knock-down larvae and the wild type, the involvement of the knocked-down Innexin in the cold nociceptive pathway was inferred. A Class III da neuron-specific tetanus toxin control was used. All eight *Drosophila* Innexins were tested with at least one RNAi construct expressed in class III da neurons. Thirteen of the fourteen total RNAi constructs resulted in significantly fewer cringers (Fischer's Two-Tailed Exact T-Test, $p<0.05$). Future studies are proposed to characterize the Innexins' role in cold nociception further.

BACKGROUND AND SIGNIFICANCE

Nociception is the perception of and response to harmful stimuli. On a cellular level, nociception may be defined as the activity in the peripheral and central nervous systems that is elicited by potentially damaging stimuli (*1*, *2*). Nociceptive responses serve to minimize tissue damage by driving avoidance of harmful stimuli. Therefore, quick, nociceptive responses have been evolutionarily selected for and passed down to a variety of organisms, from invertebrates through humans (*3*).

Transduction of a harmful stimulus initiates nociception. Specialized high threshold sensory neurons known as nociceptors transduce mechanical, chemical, or thermal stimuli (*4*). Once transduced, nociceptive inputs are then transmitted to the central nervous system, where they can be perceived, and a response can then be transmitted back out to the periphery.

A common misconception is that pain is necessarily the percept that triggers nociceptive responses*(1)*. In fact, nociception can occur in the absence of pain perception (*5*). Nociceptive input has been shown to trigger brain responses without necessarily causing pain (*6*, *7*). Nociceptive responses can still be triggered after disconnecting the nociceptors from the sensorium (the neural machinery associated with consciousness) (*2*). For example, the famous neuroscience patient H.M. (*8*) was completely unable to feel pain associated with nociceptive input after sustaining injury to his amygdala, yet, unlike patients with congenital pain insensitivity, he did not have any apparent tissue injury, implying that he retained nociceptive abilities without consciously perceiving pain (*9*). On the other hand, pain can occur in the absence of nociceptive input, such as in phantom limb syndrome (*10*). Therefore, nociception and pain perception are not synonymous. However, when nociceptors are connected to a fully

conscious central nervous system, it can be expected that pain is perceived when nociceptive pathways are activated (*2, 11*).

Certain forms of chronic pain are the result of nociceptive pathways gone awry (*5, 12*). An estimated 11.2% of the adult U.S. population suffers from chronic pain, and opioids are commonly prescribed to relieve it, with approximately 3% to 4% of the adult U.S. population prescribed long-term opioid therapy for chronic pain (*13, 14*). Opioids are highly addictive; between 8% and 12% of people prescribed opioids develop an opioid use disorder (*15-17*), and every day more than 130 people in the United States die after overdosing on opioids (*18*). It is therefore of interest to public health to precisely define the cellular and molecular pathways that nociception takes in order to identify novel targets for pain therapies.

The adaptive benefits conferred by properly functioning nociception suggest that nociception across animal phyla includes conserved cellular and physiological processes, which produce the common behavioral response of avoiding triggering stimuli (*19-21*). Since nociception is a conserved process which usually, but not necessarily, results in pain perception, invertebrates, which may or may not consciously perceive pain, can still lend insight to the pathways that pain may take in higher organisms. Indeed, there are several advantages to using invertebrates to study nociception, but despite these, invertebrates have been underutilized in nociception research (*22*). The fruit fly, *Drosophila melanogaster*, is an especially useful invertebrate for dissecting the cellular and molecular mechanisms regulating nociception (*23*).

The present study identifies novel molecular components of cold nociception in *Drosophila melanogaster* third instar larvae. Cold was chosen for the nociceptive input because the transmission of cold nociception is poorly understood and because a noxious cold behavioral response can be precisely replicated across numerous trials (*24*). The third instar stage was

chosen because earlier larval stages do not have fully developed neural circuits, particularly at neuromuscular junctions, thus impeding nociceptive responses (*25*). When third instar larvae are exposed to a 10°C plate, about half exhibit a 45-90° head and/or tail raise (HTR) and the other half exhibit a contraction (CT) of the head and tail towards the middle of the body, otherwise known as "cringing" (*24*). At the noxious temperature of 6°C, about 90% of third instar larvae exhibit the cringe response, making it an easily quantifiable and reproducible cold nociceptive response (*24*).

The location and orientation of peripheral neurons suggest a cellular path for nociception in *Drosophila* third instar larvae. Sensory dendritic arborization (da) neurons have their somas and dendritic branches located in the periphery of the larvae, while their axons travel through peripheral tissues and into the ventral nerve cord, a part of the *Drosophila* central nervous system (CNS), to form synapses (Figure 1) (*26*). These peripheral neurons are morphologically similar to vertebrate nociceptors, which synapse onto the dorsal horn of the spinal cord (*4*, *27*) (Figure 2). High-intensity optogenetic activation of class III da neurons induces the CT response, suggesting they are the peripheral neurons that mediate this cold nociceptive response (*24*).

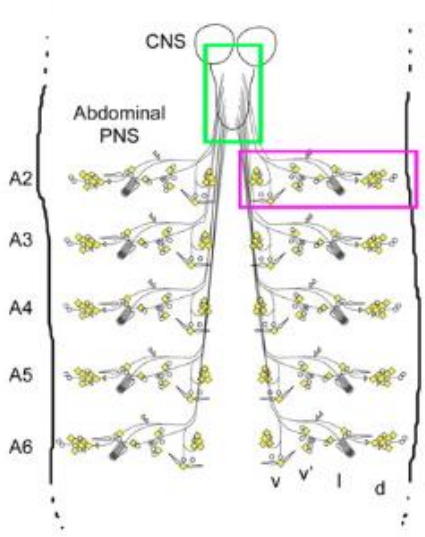

Figure 1. Schematic representation of the abdominal peripheral nervous system (magenta box) and sensory axon projections to the central nervous system (green box). Figure from (*25*).

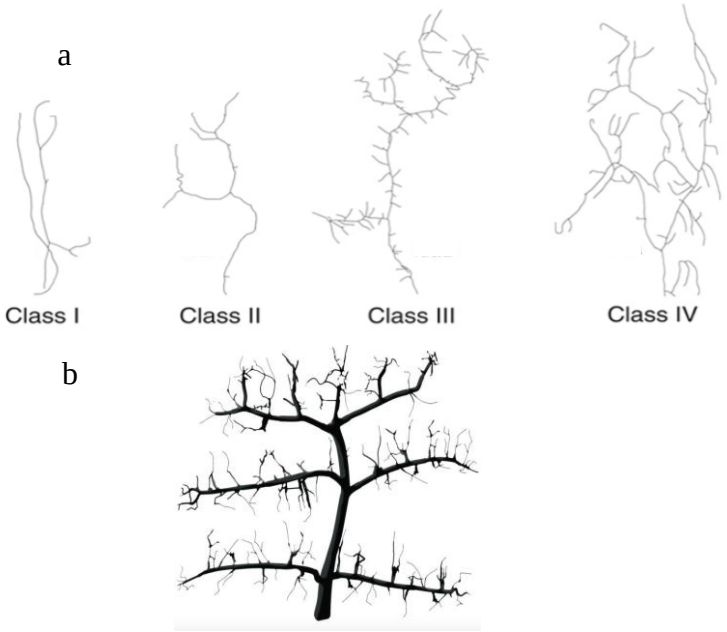

Figure 2. Nociceptor morphology. (a) Computer tracings of the branching patterns of the four classes of *Drosophila* dendritic arborization neurons. Figure modified from: (*49*). (b) A human nociceptor, the penicillate neuron of the skin. Figure from (*27*).

Molecularly, the TRP channels Trpm, NompC, and Pkd2 have been implicated in transducing noxious cold stimuli via class III da neurons (*24*). Three degenerin/epithelial sodium channel (DEG/ENaC) family members have been implicated in the subsequent propagation of these cold nociceptive signals: Ppk12, Ppk23, and Ppk25 (*28*). Other proteins that play a role in transmitting the afferent, noxious, cold stimuli and the resulting efferent responses have yet to be elucidated. I hypothesize that the vitally quick nociceptive response would function via electrical synapses since they can propagate action potentials from one neuron to the next more quickly than chemical synapses. Therefore, this study investigates the role of the invertebrate gap junction proteins, the Innexins, in cold nociception.

The *Drosophila melanogaster innexin* gene family encodes eight different Innexin family members (Table 1), which are transmembrane proteins that form hexamer hemichannels known as Innexons (Figure 3).

Table 1. *Drosophila* Innexin Family Members. The alternative names are based on descriptions of phenotypes resulting from known mutations in the genes encoding these proteins**.**

Innexin Family Member	**Alternative names**
Innexin 1 (Inx1)	Optic ganglion reduced (Ogre)
Innexin 2 (Inx2)	
Innexin 3 (Inx3)	
Innexin 4 (Inx4)	Zero population growth (Zpg)
Innexin 5 (Inx5)	
Innexin 6 (Inx6)	
Innexin 7 (Inx7)	
Innexin 8 (Inx8)	Shaking-B (ShakB)

Two Innexons on opposing neuronal membranes form an intercellular channel, which has a diameter wide enough to allow ions and small molecules to flow through it. More than one type of Innexin can form a single Innexon, and an Innexon made up of one type of Innexin can form an intercellular channel with an Innexon made up of another type of Innexin (Figure 3) (*29*).

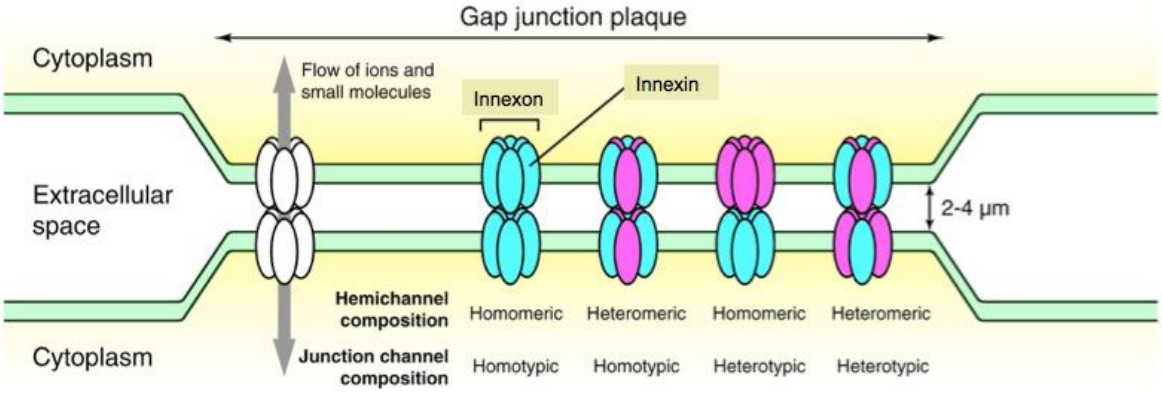

Figure 3. Gap junction structure. In invertebrates, six Innexin subunits form a hemichannel, or an Innexon. Two Innexons on opposing neuronal membranes form a channel. Several channels between adjacent neurons form a gap junction. Figure modified from (*29*).

Numerous, tightly-packed channels between adjacent neurons form a gap junction, which is the structural basis of electrical synapses.

Gap junctions allow for a near-instantaneous, large flow of ions, and thus electrical signals, between neurons. Humans have transmembrane proteins that are functionally analogous to Innexins, called Connexins, which form Connexons (*30*). Connexins do not share conserved amino acid sequences with Innexins, but they do share similar transmembrane structures (Figure 4) and they form intercellular channels in the same way (*31*). Studies suggest Innexins were the

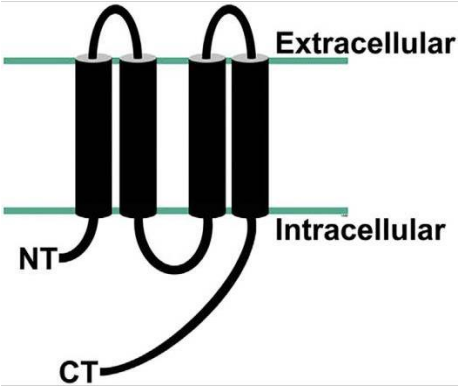

Figure 4. Membrane topology of a Connexin/Innexin/Pannexin. Transmembrane domains are depicted as cylinders that span the plasma membrane (boundaries indicated by teal line). NT, N-terminus; CT, C-terminus. Figure from (*31*).

primordial gap junction proteins, originally evolving in diploblasts for gap-junctional communication (*32*). Innexins were then inherited by protostomes and deuterostomes, while the Connexins arose *de novo* in deuterostomes (*32*). Gene duplications in the early protochordate lineage may have allowed the Connexins to replace Innexins in gap junctions, pushing the Innexins to evolve into a new subfamily, the Pannexins (*32*). Innexins and Connexins, therefore, evolved convergently to solve the problem of gap-junctional communication.

In humans, nociception has been known to occur via chemical synapses (*33*). However, this does not rule out the possibility that electrical synapses could also play a role. Despite the widespread notion that electrical and chemical synapses operate independently, there is a lot of

evidence that they functionally interact during development and adulthood in humans (*34*). Electrical and chemical synapses can function together in mixed synapses (*34*).Therefore, it is possible that electrical synapses could play a role alongside chemical ones in human nociception. The possibility also still exists that certain human nociceptive pathways whose components of transmission have yet to be identified could utilize electrical synapses alone. In support of the possibility that electrical synapses may play a role in human nociception, Connexin 36 (Cx36) appears to play a role in the anterior cingulate cortex (ACC) in another vertebrate, mice, during mechanical allodynia and thermal hyperalgesia, products of nociceptive pathways (*35*). In *Drosophila*, another vitally quick reflex, the visually elicited escape jump, utilizes Innexin 8 (Inx8), also known as Shaking-B (ShakB), to transmit the escape signal via electrical synapses in the giant fiber system (*36*, *37*). In fact, the *Drosophila* giant fiber system uses mixed chemical and electrical synapses in order to increase communication speed and fidelity between neurons (*38-40*). The main hypothesis for this study is that electrical synapses play a role in cold nociception in *Drosophila*, but this hypothesis does not exclude the possibility of electrical synapses functioning with chemical ones to transmit the cold nociceptive signal. The known role of a gap junction protein in a vitally quick reflex in *Drosophila* lends support to my hypothesis that *Drosophila* cold nociception may occur via electrical synapses, and the fact that this other vitally quick reflex might actually use mixed synapses suggests it is possible that cold nociceptive signals might be transmitted via mixed synapses as well. The fact that a gap junction protein plays a role in a nociceptive pathway in a vertebrate lends some support to the suggestion that humans may utilize electrical synapses in nociceptive pathways, either alongside the chemical ones that are known to mediate some nociceptive pathways, or alone in other, yet to be fully characterized nociceptive pathways.

Finding evidence for electrical synapses playing a role in *Drosophila* nociception would not lend direct evidence for electrical synapses playing a role in human nociception since there exists no amino acid similarity between their constituent proteins. However, under similar ancient environmental pressures, it is possible that vertebrates and invertebrates could have both ended up incorporating quick, high fidelity electrical synapses somewhere into their nociceptive pathways. Determining that Innexins play a role in the cold nociceptive pathway in *Drosophila* would provide an example of electrical synapses functioning in a nociceptive pathway, and thus would suggest electrical synapses should be explored in mammalian nociception. *Drosophila* provides a straight-forward reverse-genetic screening method to test for Innexin function in cold nociception.

In order to identify which, if any, Innexins function in *Drosophila* larvae's cold nociceptive response, the GAL4/UAS RNAi knockdown system was utilized to evaluate the effectiveness of cold nociception when a particular Innexin is down-regulated in specific neurons (*41*). The GAL4/UAS system is implemented using two different *Drosophila* lines (Figure 5). Gal4 is a transcription factor originating from *Saccharomyces cerevisiae* (*42*). This transcription factor specifically binds to a cis-acting regulatory sequence called an upstream activating sequence (UAS), thus activating expression of the downstream target sequence. The so-called driver line contains a Gal4 coding sequence inserted downstream of a promoter of an endogenous *Drosophila* gene (*43*). In the Gal4 driver lines used in this study, either a pan-da or Class III da neuron promoter is activated, and thus the Gal4 protein is expressed, exclusively in either all da neurons or only in class III da neurons. Green fluorescent protein (GFP) is also expressed under control of the same promoter as Gal4, and thus confocal imaging was used to confirm the expected driver line expression patterns. The UAS lines in this study contain

inverted repeats downstream of the UAS, which are transcribed into hairpin RNAs that are either long or short. Crossing the Gal4 driver line with the UAS line yields progeny, called the RNAi line, that express hairpin RNA in either class III or all da neurons. The presence of hairpin RNAs initiates activation of the RNA interference (RNAi) pathway, which results in sequence-specific mRNA degradation and thus knocked down expression of the target protein. Short hairpin RNAs (shRNAs) are more effective at knocking down expression of the target gene than long hairpin RNAs (*44*). In this way, the GAL4/UAS system in *Drosophila* provides a straight-forward reverse-genetic screening method to test for Innexin function in cold nociception.

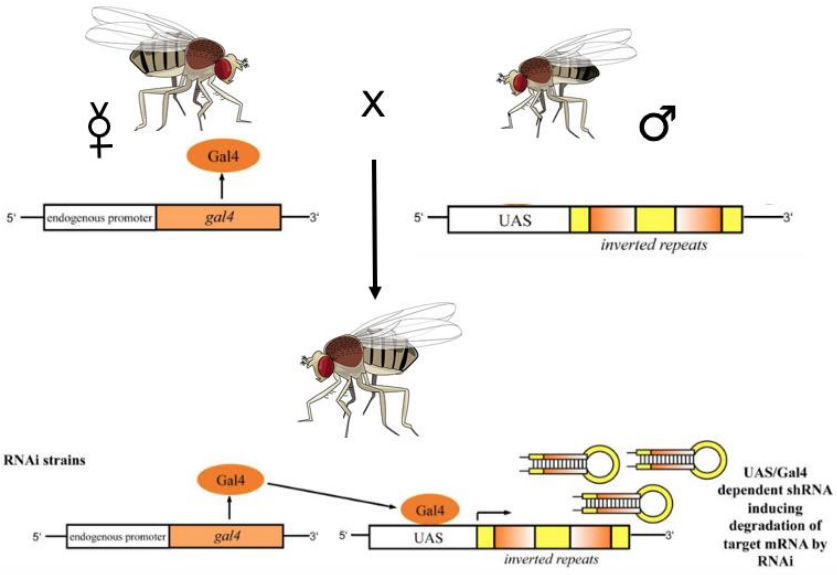

Figure 5. Gal4 driver and UAS responder cross schematic. When a GAL4 driver line is crossed to a UAS Innexin RNAi line, their progeny, express hairpin RNA in the neurons that express the endogenous gene, which *gal4* has been inserted downstream of. The presence of hairpin RNA results in degradation of target mRNA via the RNAi pathway, thus knocking down expressing of the target protein. Figure modified from (*40*).

Innexin 1 (Inx1), also known as Optic ganglion reduced (Ogre), has been shown to function in the CNS during the early and late larval periods of *Drosophila* (*45*). While Ogre does not form homomeric Innexons, it does form heteromeric Innexons when co-expressed with Inx2 in *Xenopus* oocytes (*46*). In turn, the Ogre/Inx2 heteromeric Innexons can form gap junctions with adjacent

Ogre/Inx2 Innexons (*46*). Inx2 also forms homomeric channels, which have electrophysiological properties different from the Ogre/Inx2 channels. Indeed, Ogre and Inx2 colocalize in the larval CNS (*46*). I, therefore, hypothesize that Ogre and Inx2 play a role in the larval cold nociceptive pathway. I also hypothesize that ShakB plays a role in cold nociception, since it plays a role in another vitally quick reflex, the visually elicited jump reflex, where it is known to form electrical synapses in the giant fiber system (*36*, *37*).

METHODS

Stocks

Fly stocks were obtained from the Bloomington *Drosophila* Stock Center, the Vienna Drosophila Resource Center, and Dan Cox's lab at Georgia State University (Table 2). Gal4 driver lines were crossed to UAS responder lines to produce the desired genotype (Table 3, Figure 5). Third instar larvae of the desired genotype were selected for analysis. To control for false positive/negative results, when possible, more than one UAS RNAi construct was tested for each *innexin* gene.

Oregon R was used as the wild type line. The Gal4 Class III da neuron driver was 19-12-Gal4 (*47*) and the pan-da neuron driver was 21-7-Gal4 (*48*). Both driver lines express the Gal4 protein along with green fluorescent protein in the neurons to which they are specific. A total of fifteen UAS RNAi constructs were tested for the experimental trials (Table 2). A UAS line carrying a tetanus toxin (TNTE) transgene had been utilized as the cold behavioral assay positive control in a previous project in this lab, which explored the involvement of DEG/ENaC channels in the cold nociception pathway (*28*). Subsequently, this line was used for the purpose of the positive control in this project, in order to reveal cringe inhibition when either Class III da neurons or all da neurons' functionalities are impaired.

Table 2. Stocks

Function	Stock Number	Genotype	Description	Alternative name
Wild Type	N/A[1]	Oregon R	Wild Type	OR
Gal4 Class III da neuron driver	N/A[1]	19-12-Gal4, UAS-mCD8::GFP	Class III specific driver/imaging	19-12
Gal4 pan-da neuron driver	N/A[1]	21-7-Gal4, UAS-mCD8::GFP	Pan-da driver/imaging	21-7
Control Responder	N/A[1]	UAS-TNTE	Tetanus Toxin	UAS TNTE
RNAi Responders	JF 02595[2]	*y[1] v[1]; P{*TRiPJF02595}attP2	*ogre* long hairpin RNA	UAS *ogre* RNAi
	JF 02446[2]	*y[1[v[1];* P{TRiPJF02446}attP2	*inx2* long hairpin RNA	UAS *inx2* RNAi
	HM S02481[2]	*y[1] sc* v[1];* P{TRiPHMS02481}attP2	*inx2* shRNA	UAS *inx2* RNAi
	HM 05245[2]	*y[1] sc* v[1];* P{TRiPHM05245}attP2	*inx3* long hairpin RNA	UAS *inx3* RNAi
	KK 106268[3] (VDRC #108913)	UAS-inx3-RNAi P{KK106268}	*inx3* long hairpin RNA	UAS *inx3* RNAi
	GL 00447[2]	*y[1] sc* v[1];* P{TRiPGL00447}attP2	*zpg* long hairpin RNA	UAS *zpg* RNAi
	JF 02753[2]	*y[1] v[1]; P{*TRiPJF02753}attP2	*zpg* long hairpin RNA	UAS *zpg* RNAi
	JF 02877[2]	*y[1] v[1];* P{TRiPJF02877}attP2	*inx5* long hairpin RNA	UAS *inx5* RNAi
	KK 103391[3] (VDRC #102814)	UAS-inx5-RNAi P{KK103391}	*inx5* long hairpin RNA	UAS *inx5* RNAi
	JF 02168[2]	*y[1] v[1];* P{TRiP.JF02168}attP2	*inx6* long hairpin RNA	UAS *inx6* RNAi
	GD 3692[3] (VDRC #8638)	UAS-inx6-RNAi P{GD3692}	*Inx6* long hairpin RNA	UAS *inx6* RNAi
	JF 02066[2]	*y[1] v[1];* P{TRiP.JF02066}attP2	*Inx7* long hairpin RNA	UAS *inx7* RNAi
	KK 112684[3] (VDRC #103256)	UAS-inx7-RNAi P{KK112684}	*Inx7* long hairpin RNA	UAS *inx7* RNAi
	JF 02603[2]	*y[1] v[1];* P{TRiP.JF02603}attP2/TM3, Sb1	*ShakB* long hairpin RNA	UAS *ShakB* RNAi
	GD 7794[3] (VDRC #24578)	UAS-shakB-RNAi P{GD7794}	*inx7* long hairpin RNA	UAS *ShakB* RNAi

Stocks sources:
1=Dan Cox, Georgia State University
2=Bloomington Drosophila Stock Center
3=Vienna Drosophila Resource Center

Confocal Microscopy

Confocal images of third instar larvae from the driver lines were acquired in order to visualize where the Gal4 protein was being expressed. The expression pattern of the *gfp* transgene served as a proxy for the *gal4* transgene expression pattern since they are under control of the UAS responder promoter. The *Drosophila* driving 19-12 Gal4 expression should be specific to Class III da neurons while the *Drosophila* promoter for 21-7 drives expression in all da neurons (see Results below). Once expressed, the GFP is localized to the cell membrane, permitting visualization of neuronal expression.

Third instar larvae collected directly from the homozygous 21-7 pan-da neuron driver line were imaged. Due to excessive non-specific GFP expression in the homozygous larvae, the 19-12 Class III da neuron driver line was crossed to the wild type OR line and the heterozygous third instar larvae progeny were imaged. Live confocal imaging was performed according to a protocol provided by Dr. Dan Cox (personal communication). A small drop of 1:5 ethyl ether:halocarbon oil solution was placed on both ends of a standard 1x3" microscope slide. Two 22x22 mm coverslips were placed on top of the small droplets and moved slightly side to side until they were difficult to move. Next, a third instar larva was briefly washed with water in a 9-well plate and placed on a kimwipe for brief drying. The dried larva was placed in the middle of the 1x3" slide and a few large drops of ethyl ether:halocarbon oil solution were placed on the larva, and one small drop of solution was placed on each 22x22 mm coverslip. Once the larva was oriented in a relatively straight position, a 24x50 mm coverslip was placed on top of the larva and the two smaller coverslip bridges and moved gently side to side until the larva was completely flat and straight.

Images were acquired on a Nikon C2si laser scanning confocal microscope, using a PlanApo 10x (0.45NA) objective. GFP was excited by the 488 nm line of an Argon Ion laser and detected on a PMT with a 525/50 filter. The pixel resolution was adjusted to 1.25 μm/px; slices in z-stacks were acquired every 3.00 μm. Images were acquired with 2x averaging to reduce noise. Images have been stitched from multiple fields-of-view and are maximum intensity z-projections of selected z-slices.

Crosses

Oregon-R flies provided the wild-type control for the larval response in the cold behavioral assay (Table 3). Quantification of cringing inhibition when either Class III da neurons' or all da neurons' functionality was impaired was determined by driving tetanus toxin expression with the appropriate Gal4 Driver (Tetanus Toxin or "TNTE" control, Table 3). This was considered a negative control because there was no inhibition in the cringe response. More specific negative control crosses were utilized for comparative analysis of each RNAi construct (Table 3). RNAi non-expressed controls were made by crossing the wild type (OR) line with the appropriate *innexin* UAS RNAi.

Table 3. Crosses, Genotypes, and Function of Larvae for Cold Plate Behavioral Assays

♀	♂	**Function in Assay**
OR	OR	Wild Type control
19-12	UAS TNTE	Tetanus Toxin control in Class III da neurons
21-7	UAS TNTE	Tetanus Toxin control in all da neurons
19-12	UAS RNAi	Experimental knockdown in Class III da neurons
21-7	UAS RNAi	Experimental knockdown in all da neurons
OR	UAS RNAi	Non-expressed RNAi controls

To generate the desired genotypes, 20 virgin females were crossed with 10 males. Crosses were performed in 6-oz bottles containing 50mL of standard cornmeal/molasses food. All bottles were incubated at 25°C for 6-8 days. Third instar larvae were identified as those actively crawling on the walls of the bottles and were noticeably larger than the first and second instar larvae, which remained in the food.

Reverse Genetic Screening by Cold Plate Behavioral Assay

The cold plate behavioral assay setup consisted of a thermocycler, a Nikon 5200 camera mounted above and pointed towards the thermocycler's sample block, a concentrated light source illuminating the sample block horizontally, and a black-painted aluminum plate, which was about the size of the thermocycler sample block (Figure 6).

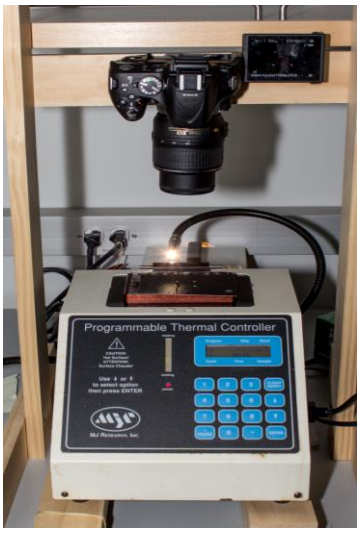

Figure 6. Cold plate behavioral assay setup. A Nikon 5200 is mounted directly above the sample block of a PTC-100 thermocycler. Larvae are placed on a misted aluminum plate, which is placed atop the flooded sample block. Located in a dark room, a concentrated light source allows for illumination of the larvae without much illumination of the water droplets on the aluminum plate. Photo taken by Ben Williamson.

To begin the cold behavioral assay, the thermocycler was set to 6°C and the wells were filled with deionized water. 6°C was used because 90% of third instar larvae exhibit the cringe response to this stimulus (*24*). Four third instar larvae were collected from the walls of a bottle

with a small, wet, pointed paintbrush, briefly deposited into a well of a 9 well plate filled with deionized water, then dried on a kimwipe. The black aluminum plate was misted with deionized water via a standard spray bottle, and the rinsed larvae were placed in quadrants on the misted plate with the paintbrush. Video recording from the Nikon was started, and the larvae-bearing plate was placed and held on the 6°C sample block for 30 seconds. The temperature of the sample block with the aluminum plate on top was routinely verified over the course of several videos with an infrared thermometer. This procedure was repeated until quality processed videos of 100 individual larvae were obtained.

To correct for subtle differences in performance of the assay, each lab member performed both the non-expressed control and experimental knockdown cold behavioral assays for a specific *innexin* RNAi genotype along with a wild type control. In every case, the average cringing behavior pattern of each experimental control was compared to that of the wild type control group assayed by the lab member. Statistically, in every case, the experimental control did not differ significantly from the OR wild-type control ($P>0.05$, Fischer's Two-tailed Exact test; data not shown). This verified that the assays were consistently performed, although slight differences were observed in peak cringing levels and the time at which the peak cringe occurred.

Video Processing and Analysis

MOV formatted videos were converted to AVI, which is compatible for import into Image J (*49*). Image J was then used to process the videos and convert into numerical data so "percent cringe" over time could be calculate.

The first Image J function used was to convert each video to grayscale (Figure 7A). The first frame in which the plate comes into contact with the cold surface was then determined visually and set as the first frame used in data analysis. The following 15 seconds of the video were analyzed. The threshold function was then used to create the clearest possible larval silhouettes in all frames. Once the silhouettes were created, the video was converted to binary form, which showed a black silhouette of the larva against a white background. Once in binary form, the skeletonize function was used to transform the larvae into linear form. Each larva was selected according to their quadrant and particles were analyzed for length data (length corresponds to cringing behavior). The length was collected via the area function under particle analysis.

Length data (read as area in Image J) was then imported into Excel for analysis (Figure 7B). The desired form of this data was "percent cringe" for each frame of the video. Percent cringe is defined as the percent change in length from the maximum length of the larva. The equation used to calculate this was: ((MAX length – length in the respective frame)/MAX length)*100. The average percent cringe of 100 larvae per sample was calculated for each frame of each video, resulting in an average percent cringe over time graph (Figure 7C).

a

b

Time (s)	Length (# of pixels)	% Cringe
0.0	80	0
0.1	78	2.5
0.2	77	3.75
0.3	77	3.75
0.4	68	15
0.5	59	26.25
0.6	62	22.5
0.7	55	31.25
0.8	59	26.25
0.9	58	27.5
1.0	54	32.5
1.1	51	36.25
1.2	49	38.75
1.3	48	40
1.4	48	40
1.5	47	41.25

c

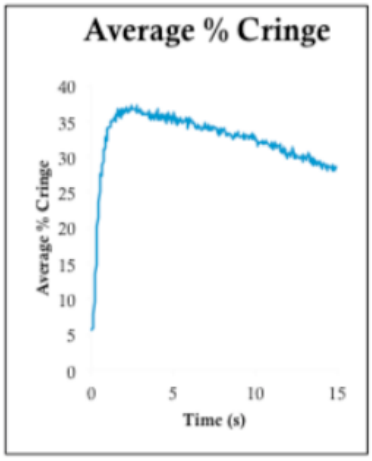

Figure 7. Image processing and calculation of percent cringe. (a) The first row shows an image of the raw video. Next, the threshold function is used to separate the pixels based on brightness, shown in the second row. The pixels are then converted to binary form (third row), which separates them into black and white based on the previously determined threshold. Finally, the larvae are converted to linear form via the skeletonize function (fourth row). The larva in this figure is a wild type Oregon R at 0s (before cringing) on the left and 1.5s (during cringing) on the right. (b) The percent cringe data is calculated from the pixel data. (c) A full length (15s) larvae video plotted as average percent cringe-over-time. Figure from: (*28*).

Data Normalization and Statistical Analysis

In order to compare average cringing behavior between the different *innexin* RNAi genotypes, each larva was classified as either a cringer or a non-cringer (*24*). The threshold for this distinction was determined by comparing the data for the expressed RNAi to the relevant experimental control group for its genotype.

First, the time at which the control group reached its maximum average percent cringe was found. A 3-second window was established around this time. Then, the maximum percent cringe that each control larva reached during this 3-second window was found. From this series of maximum cringe percentages within the 3-second window, the average and standard deviation

were calculated. The standard deviation was multiplied by 1.5 and subtracted from the average to obtain the threshold associated with that control.

A 3-second window was established in the same way for each experimental group. The maximum percent cringe that each experimental larva reached during this 3-second window was compared to the threshold established by the control group. Larvae that reached a maximum percent cringe during the 3-second window equal to or greater than the threshold were classified as cringers. Larvae that did not reach the threshold during the 3-second window were classified as non-cringers.

The number of non-cringers in each experimental group was compared to the number of non-cringers in each control group using the Fischer Two-Tailed Exact Test in Excel (α=0.05).

RESULTS

Confocal Images

Confocal imaging confirmed the assumed expression patterns of the Gal4 driver lines. The heterozygous 19-12-Gal4/+ third instar larvae expressed GFP in Class III da neurons (Fig. 8a) and the homozygous 21-7-Gal4 third instar larvae expressed GFP in all da neurons (Fig. 8b) (*50*). About 10 larvae of each driver genotype were imaged to confirm these expression patterns. The expression of GFP reveals that the neurons are arranged in a repeated segmental pattern along the length of the larvae. Close up images of single larval segments illustrates the differences in driver expression (Fig. 9). Class III da neurons express GFP in the stereotypical arborization pattern. The 21-7-Gal4 driver expressed in all da neurons. These neurons underlie

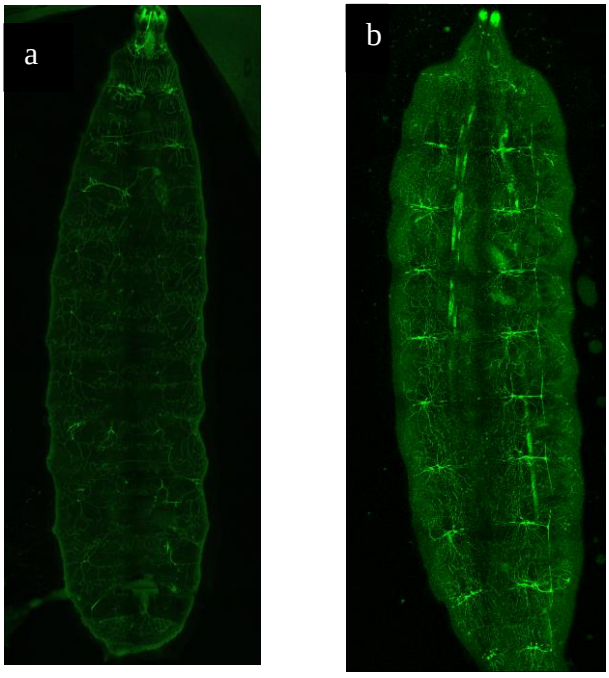

Figure 8. Full-body confocal images of the larvae expressing either 19-12-Gal4 or 21-7-Gal4. (a) A heterozygous 19-12-Gal4/+ third instar larva expressing GFP only in Class III da neurons. (b) A homozygous 21-7-Gal4 third instar larva expressing GFP in all sensory da neurons. Some non-specific GFP expression can be seen.

the epidermis in a non-overlapping pattern as demonstrated in previous studies (*51*). Thus, the UAS *innexin* RNAi constructs were expressed in the expected da neurons by each driver.

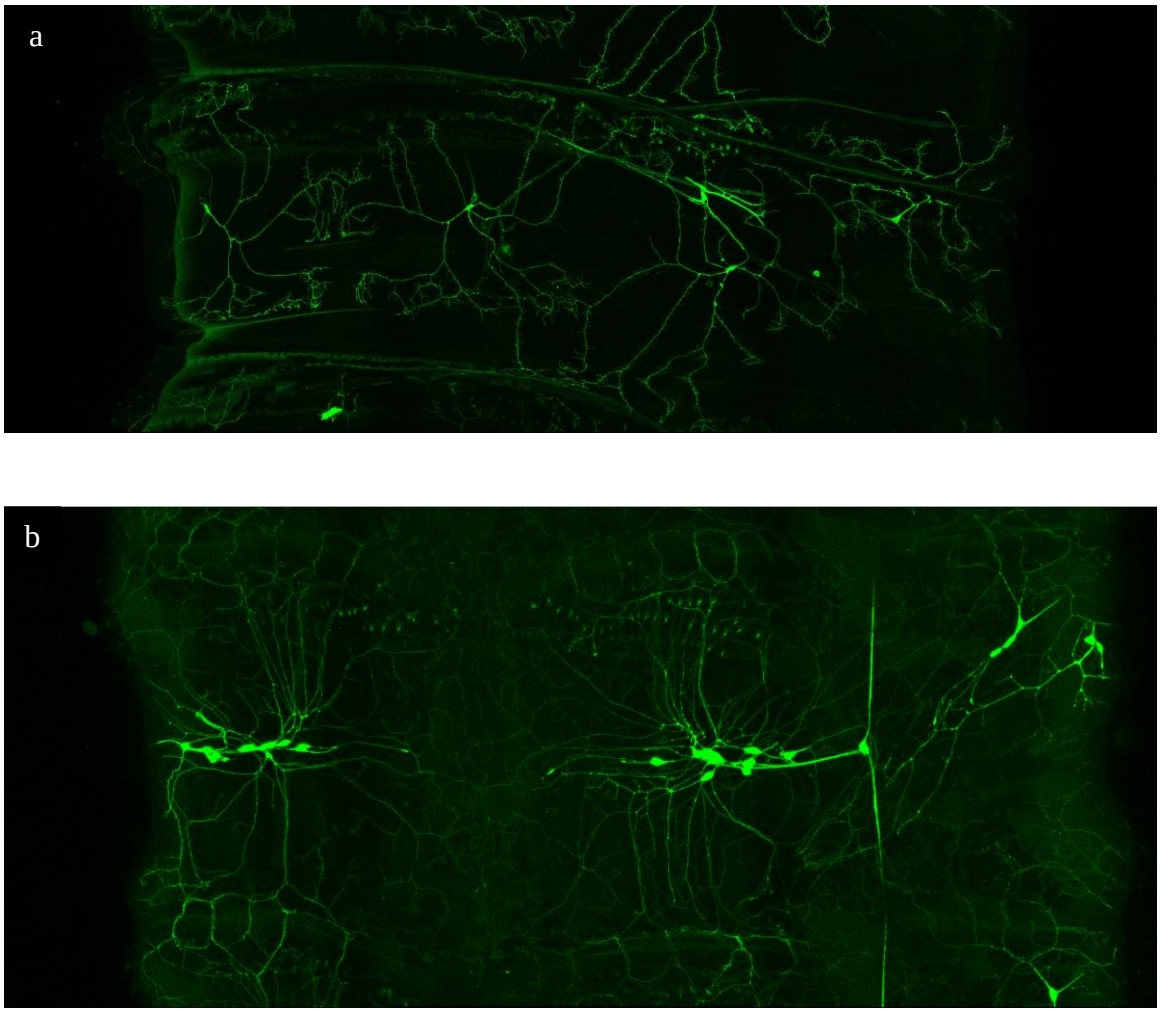

Figure 9. Close-up confocal images of a single segment of larvae expressing their respective drivers. (a) The class III da neurons in a 19-12/+ larva. (b) A homozygous 21-7 larva expresses GFP in Class I, II, III, and IV neurons.

Cold Behavioral Assay Data Analysis

In order to identify which, if any, Innexins function in *Drosophila* larvae's cold nociceptive response, cold behavioral assays were performed on larvae that had a particular Innexin down-regulated in specific neurons. The results of each cold behavioral assay were

plotted as average percent cringe-over-time connected scatter plots. An example is shown for tetanus toxin (TNTE) expressed in Class III da neurons (Figure 10). At 5 seconds, the wild type control and the non-expressed tetanus toxin control peak cringed 36.8% and 38.1% respectively. There is no significant difference between these cringe responses ($P<0.01$, Two-tailed Fisher Exact Test). Conversely, larvae in which tetanus toxin is expressed in class III da neurons cringed only 24.1% at 5 seconds, which is significantly lower than the peak cringe values of both the wild type and non-expressed tetanus toxin controls ($P<0.001$ for each comparison). Expressing tetanus toxin in all da neurons was lethal, as no progeny resulted from crossing the UAS TNTE line with the 21-7 driver.

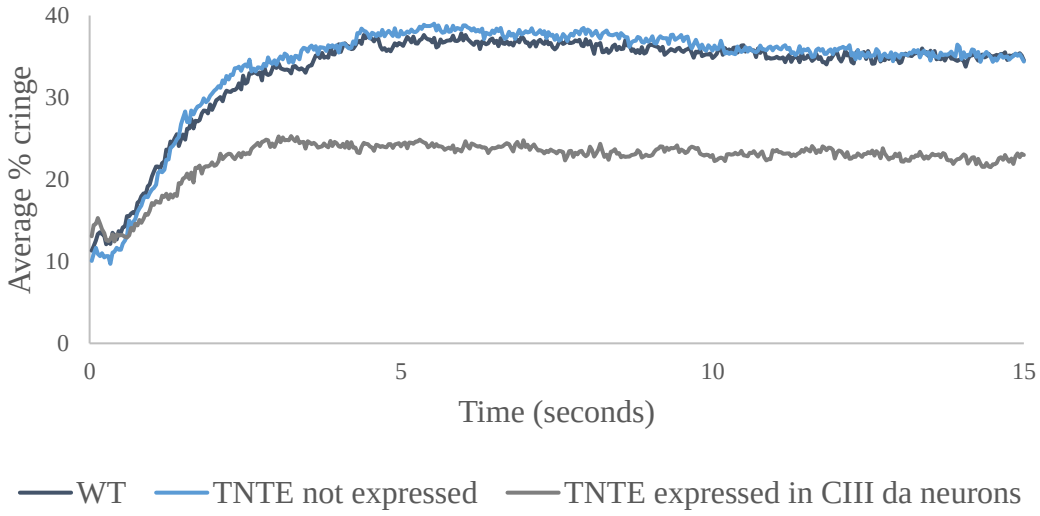

Figure 10. Cold behavioral assay results of tetanus toxin (TNTE) expressed in Class III da neurons. The average percent cringe of 100 larvae for each condition is plotted over time. The behavioral assay was performed at 6°C.

After plotting cold behavior as average percent cringe-over-time, each individual larva within the pool of 100 larvae was classified as a cringer or a non-cringer based on a threshold set by the relevant control group. Since cringing peak responses are variable between larvae in every group tested, including controls and between genotypes, this normalization allows direct comparisons between genotypes. For each experimental control, the averaged peak cringe was

determined. A three-second window flanking this value was determined and 1.5 standard deviations of the average peak cringe within this window was calculated (Fig. 11).

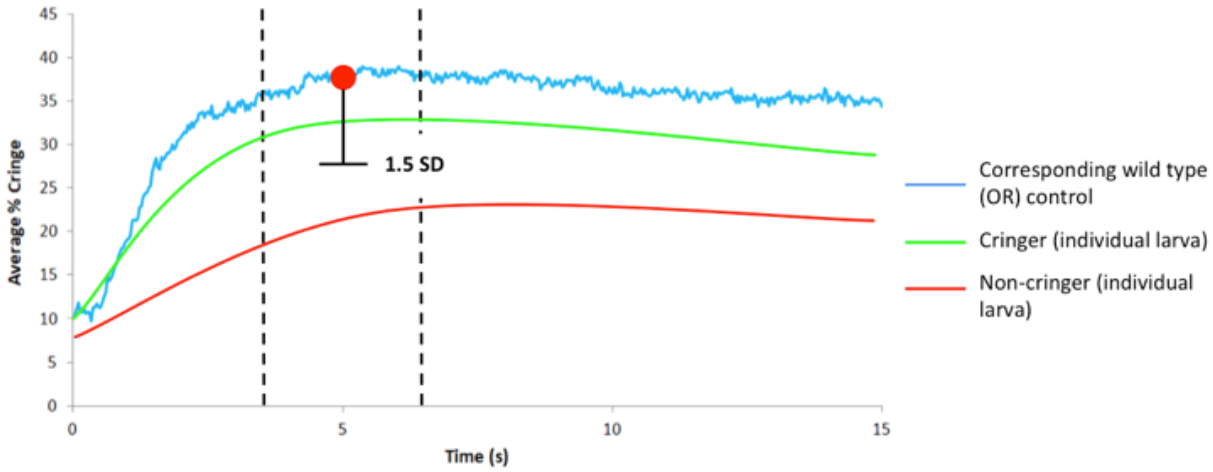

Figure 11. Diagram representing how thresholds for cringers versus non-cringers were established. The jagged blue line represents the average cringe-over-time plot for the relevant control group, wild-type OR in this case. The smooth red and green lines each represent the cringing response of a hypothetical single larva belonging to an experimental knockdown group. Diagram created by Kendyl Combs.

Individual experimental larvae were then compared to the control within this window. If the larva's peak cringe fell within the 1.5 standard deviations, it was classified as a cringer. Those falling below this threshold were classified as non-cringers. Subsequently, the number of non-cringers in each group was calculated and plotted in a bar graph, with the x-axis being the percentage of larvae that were classified as non-cringers in each group (Figure 12). The Fischer Two-Tailed Exact Test was used to determine if the difference in the number of non-cringers in the experimental group differed significantly from the control group.

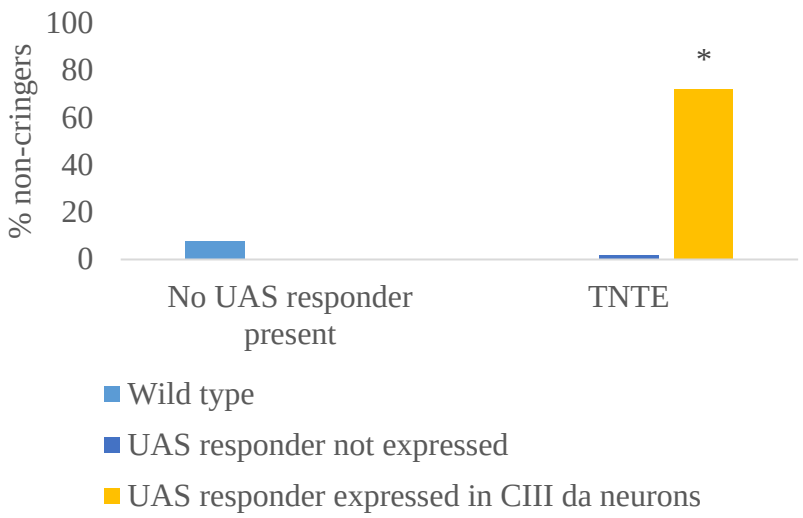

Figure 12. Cold behavioral assay results plotted as percent non-cringers. The x-axis includes which UAS responder is present in each cluster of bars. The legend describes the expression patterns for each UAS responder. The percentage of non-cringers in the non-expressed TNTE control group was compared to that of the wild type group ($p>0.1$), and the percentage of non-cringers in the expressed TNTE group was compared to that of the non-expressed TNTE group. The asterisk indicates a significant difference between the percentage of non-cringers in the expressed TNTE and non-expressed TNTE groups ($p<10^{-27}$).

The results of the cold behavioral assays for each Innexin RNAi stock were plotted on individual cringe-over-time graphs. These graphs include results for the group in which the UAS RNAi construct was present but not expressed, the group in which the UAS RNAi was expressed in Class III da neurons, the group in which UAS TNTE was expressed in Class III da neurons (for comparison purposes), and the group in which the UAS RNAi was expressed in all da neurons, when available (Figure 13).

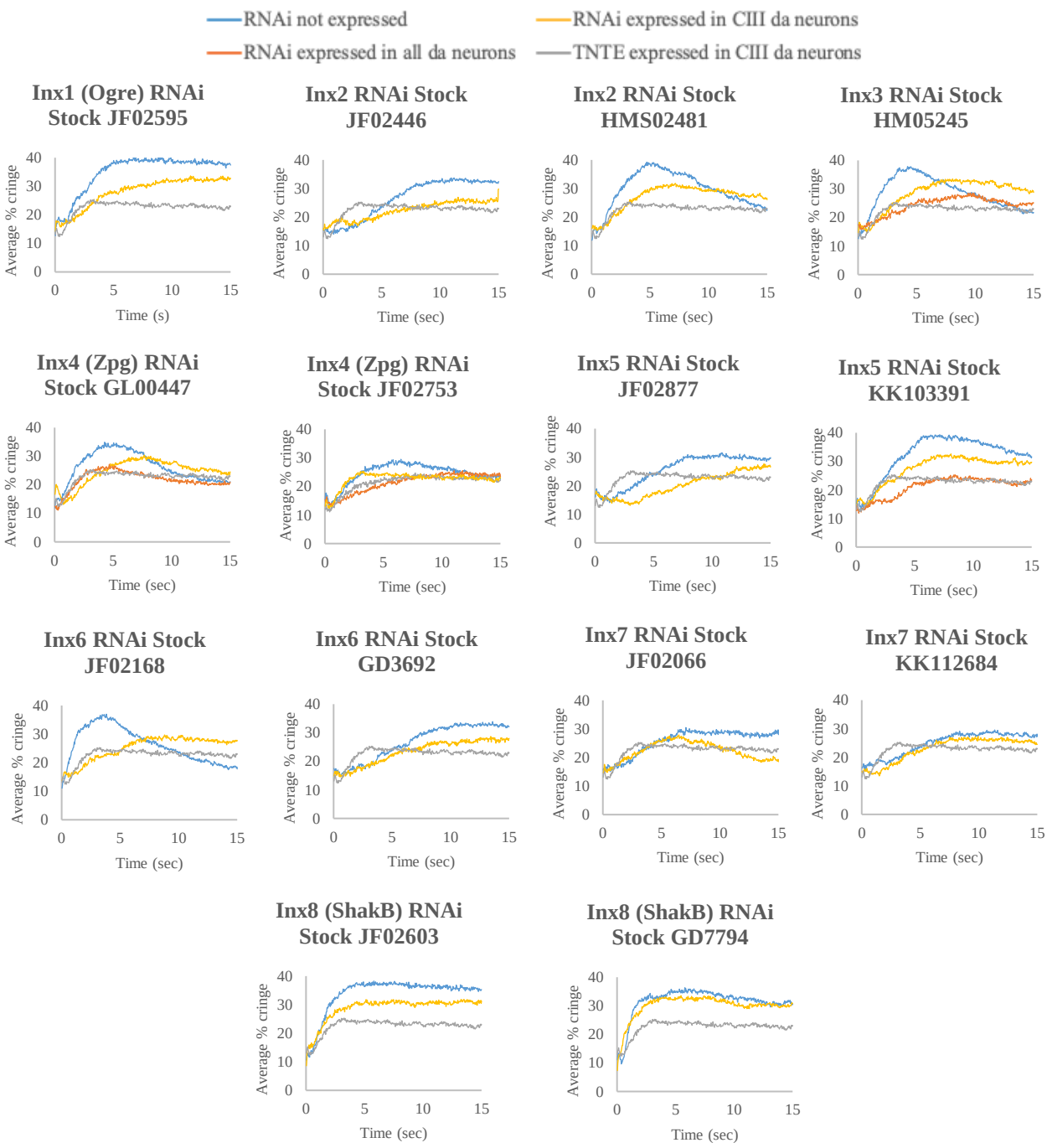

Figure 13. Effect of *innexin* RNAi expression on the cringe response. The name of the UAS RNAi stock tested and the Innexin it targets are listed above each cringe-over-time graph. The gray plot depicts the cringe response when TNTE is expressed in Class III da neurons and this is plotted in each graph. Blue plots are the experimental controls when the *innexin* RNAi is not expressed. Every graph plots the expression of the corresponding *innexin* RNAi Class III da neurons (yellow). Expression of *innexin3*, *innexin4*, and *innexin5* [KK103391] RNAi in all da neurons is also plotted (orange).

In order to directly compare all genotypes and to account for slight variations in the data, all data were normalized to determine the number of non-cringers in each group. Impairment of the wild type cringe response results in a significant increase in the number of non-cringers within an experimental sample. The normalized data for each genotype was plotted as a bar graph and the percentages of non-cringers in the expression groups were compared statistically to the control groups (Figure 14).

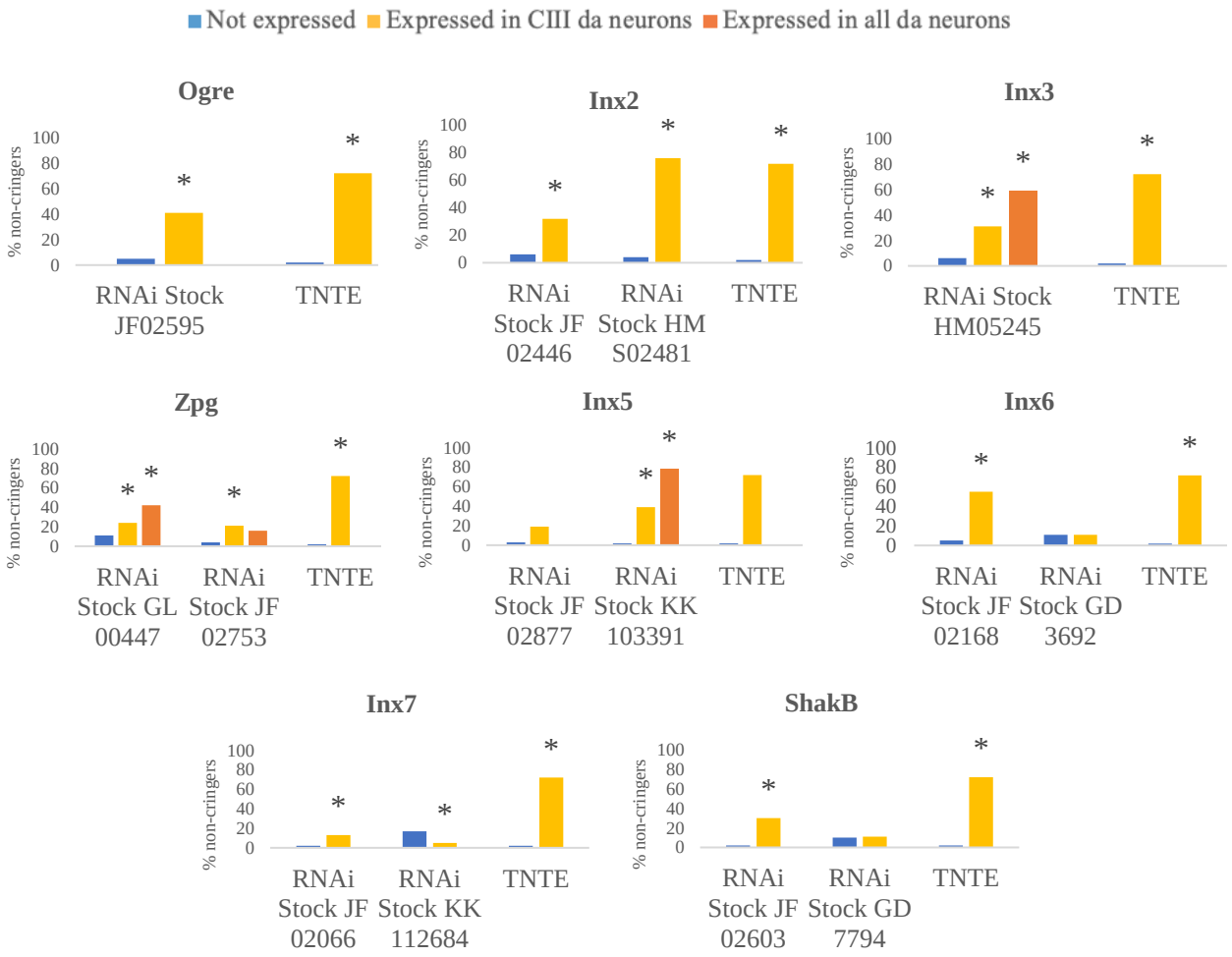

Figure 14. Inhibition of cringing visualized as the percent of non-cringers after RNAi knockdown. Each larva was determined to be a cringer or non-cringer (see Methods) for both the expressed RNAi experiments (yellow bars expression in Class III da neurons, orange bars expression in all da neurons) and its corresponding experimental control (blue bars). Experimental *innexin* knockdown trials (yellow and orange) are compared to non-expressed RNAi trials (light blue). Significant differences between the percentage of cringers in the experimental knockdown and non-expressed RNAi trials are indicated by asterisks above the experimental knockdown bar (Fischer's Two-Tailed Exact Test, $p<0.05$).

The average peak cringe for the non-expressed RNAi controls ranged from 29.5-40.3% with a standard deviation of 3.9% (Figure 15a). The range of the average peak cringe for the groups of larvae expressing *innexin* RNAi in Class III da neurons was overall lower than that of the non-expressed RNAi controls, at 25.5-33.6% with a standard deviation of 2.7%, and the range of the average peak cringe for the groups of larvae expressing *innexin* RNAi in all da neurons was overall even lower at 24.7%-28.6% with a standard deviation of 1.8%.

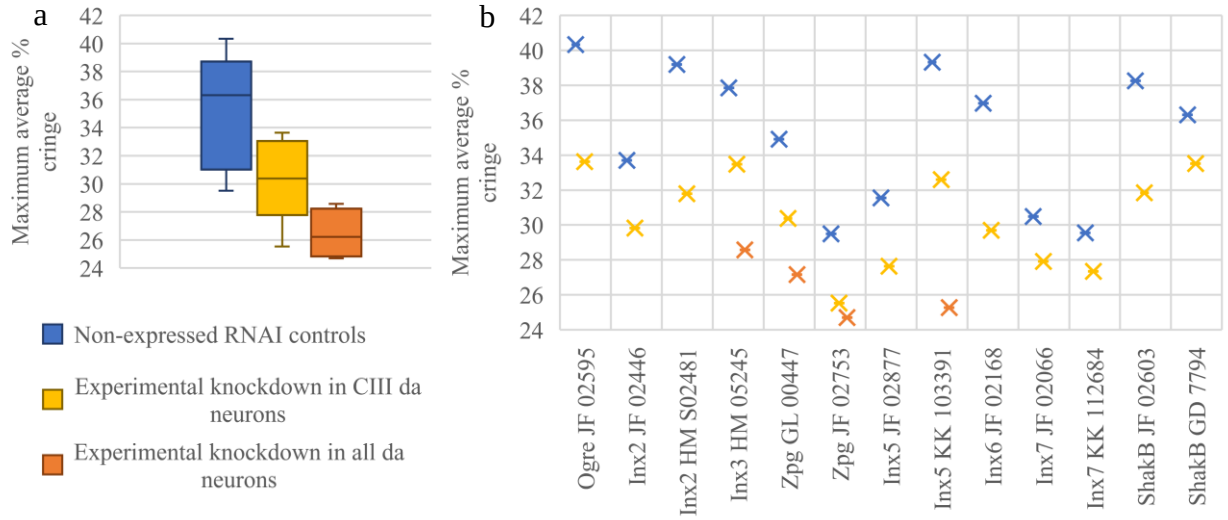

Figure 15. Box plots depicting the ranges of average maximum percent cringe values. Short, bottom-most line=minimum value; lower part of box=first quartile; line dividing the box=median; upper part of box=third quartile; short, upper-most line=maximum. (a) Maximum average percent cringe ranges for each RNAi expression pattern. (b) Maximum average percent cringe values for each RNAi construct. Yellow, expression in Class III da neurons; Orange, expression in all da neurons; blue, experimental control.

The Inx1 (Ogre) Class III da neuron knockdown larvae reached one of the higher average peak cringe values, relative to the other Class III da neuron *innexin* knockdown groups, along with the group of larvae expressing the only Inx3 RNAi construct, the Inx5 KK103391 RNAi construct, and the Inx8 (ShakB) GD7794 RNAi construct (Figure 15b). However, normalization by comparing the experimental RNAi knockdown peak cringe values to that of the non-expressed RNAi controls revealed that the Class III Ogre, Inx3, and Inx5 KK103391 knockdowns still significantly inhibited cringing (Fig. 14). The Class III da neuron *innexin* knockdown group that reached the lowest average percent cringe out of all the Class III

knockdown groups was the group expressing the Zpg JF02753 RNAi construct, with the groups expressing the Inx5 JF02877 construct and the two Inx7 RNAi constructs reaching the next lowest average percent cringe values (Fig. 15b). However, once again, normalization of the data reveals that despite these low average maximum percent cringe values, some of these knockdowns did not result in significantly more non-cringers compared to the non-expressed RNAi controls (Fig. 14). Particularly, the Inx5 RNAi construct JF02877 did result in more non-cringers compared to the non-expression control, and the Inx7 KK112684 construct actually resulted in significantly fewer non-cringers compared to its non-expression control (Fig. 14).

The *innexin* Class III da neuron knockdown groups, for the most part, reached their average maximum percent cringe values later than both the non-expressed RNAi controls and the *innexin* pan-da neuron knockdown groups (Figure 16a). The groups that expressed RNAi responders Inx2 JF02446, Inx5 JF02877, and ShakB JF02603 peaked latest (Figure 16b). The Class III da neuron *innexin* RNAi groups that peaked earliest were Inx2 HMS02481, Inx7 JF02168, and ShakB GD7794 (Figure 16b).

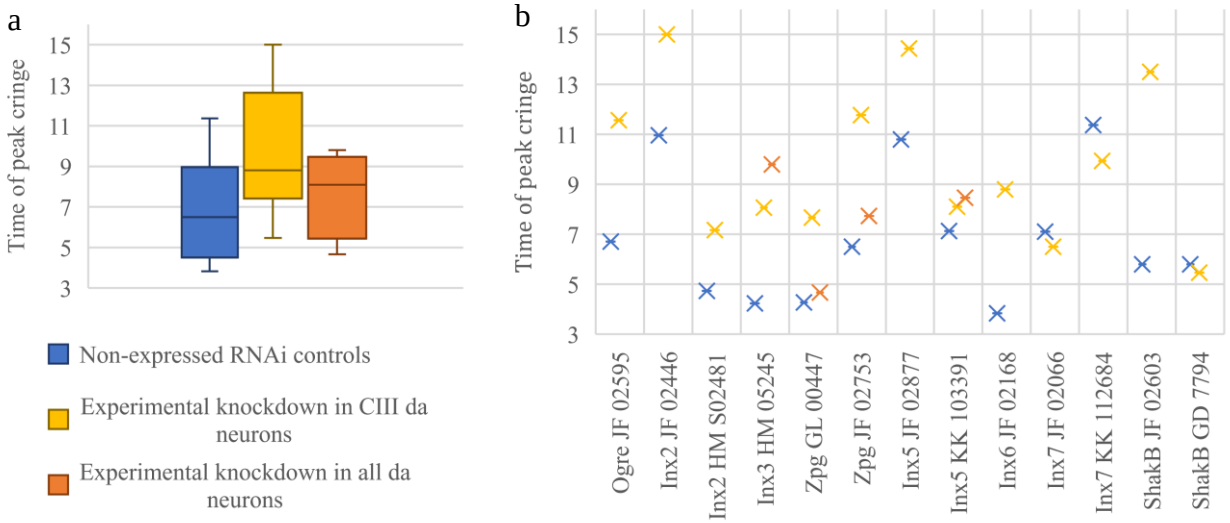

Figure 16. Box plots depicting the ranges of times at which the average cringe values reached a peak. (a) Time of maximum average percent cringe ranges for each RNAi expression pattern. (b) Times of maximum average percent cringe for each RNAi construct and expression pattern.

When expressed in Class III da neurons, the RNAi construct that resulted in the greatest inhibition of cringing, as demonstrated by percent non-cringers, was the one short hairpin RNA that was tested, Inx 2 RNAi stock HMS02481 (Figure 14). At 76%, this *innexin* Class III da neuron knockdown group had more non-cringers than the Class III da neuron tetanus toxin control, which had 72% non-cringers (not significantly different, $p>0.6$).

The Inx5 JF02877 Class III da neuron knockdown average percent cringe-over-time curve is markedly different from all of the other Class III da neuron knockdown curves (Fig. 13). The typical shape of the cringe-over-time plots was a rapid increase to a peak average cringe, then a plateau, while the Inx5 JF02877 Class III da neuron knockdown average percent cringe-over-time curve demonstrated an average lengthening first, followed by a gradual increase in average cringing for the rest of the assay. Of all of the other curves, the Inx2 JF02446 Class III da neuron knockdown curve appears the most similar to this markedly atypical Inx5 JF02877 curve, with a small initial average relaxation followed by a gradual increase in average percent cringe (Fig. 13). The Inx6 Class III da neuron RNAi-expressed curves also showed an atypical gradual increase in average percent cringe, but without an initial average elongation (Fig. 13).

The two Inx4 (Zpg) Class III-expressed RNAi constructs resulted in a rapid initial average relaxation followed by the stereotypic quick average cringing and plateau (Fig. 13). However, the Zpg RNAi non-expression control curves followed a similar pattern.

Individual knockdown of each Innexin in Class III da neurons resulted in significantly more non-cringers with at least one of the UAS RNAi responder lines (Figure 14). Innexins 5, 6, and 8 (also known as ShakB) were the Innexins that had conflicting percent non-cringer results with the two UAS RNAi responder constructs that were tested against them.

When expressed in all da neurons, only one UAS *innexin* RNAi responder did not result in significantly more non-cringers than the non-expressed RNAi control, Zpg RNAi stock JF02753 (Figure 14).

DISCUSSION

Innexins Function in *Drosophila* Cold Nociception

The general hypothesis for this study was that electrical synapses, and thus one or more of the Innexin proteins that compose electrical synapses, function in the cold nociception pathway of *Drosophila melanogaster* third instar larvae. The predicted experimental result based on this hypothesis was that knocking down at least one of the Innexins in the neurons that mediate cold nociception would result in an inhibited cold nociceptive response, demonstrated by significantly more non-cringers in the knockdown group.

Indeed, knocking down at least one Innexin did result in significantly more larvae that classified as non-cringers in response to noxious cold, supporting the hypothesis that electrical synapses play a role in the *Drosophila* larval cold nociception pathway (Figure 14).

Surprisingly, knocking down every single Innexin individually in Class III da neurons with at least one RNAi construct resulted in significantly fewer cringers (Fig. 14). This could mean that every Innexin plays a role in the cold nociception pathway, or that knocking down Innexins in Class III da neurons negatively affects the larvae's general ability to cringe. The latter explanation implies that the cringe response triggered by the cold plate assay used here is not truly a nociceptive response, but rather a more general, muscular response to cold. This is probably not the case for several reasons. First, a known non-nociceptive physiological response to cold temperatures in *Drosophila* is chill coma, in which muscle function is temporarily impaired by low temperatures (*52*). The robust wild type cringe response to the noxious temperature of 6°C clearly overrides the physiological problem of chill coma, as a vitally important reflex such as nociception would be expected to do. Second, strong optogenetic

activation of Class III da neurons reproduces the cringe response at room temperature (*24*). The strength of the optogenetic stimulation needed to reproduce the cringe response supports the hypothesis that the cringe behavior is a nociceptive response. This recreation of the cringe response via optogenetic activation of Class III da neurons also demonstrates that activation of Class III da neurons is sufficient for the cringe response. In addition, previous studies and the tetanus toxin control prove that Class III da neurons are necessary for the cringe response (*24*). Taken together, these pieces of evidence suggest the cold-evoked cringe response is indeed nociceptive. Due to the evidence supporting the notion that the cold-evoked cringe response is indeed nociceptive, and because the neurons the Innexins were knocked down in are both necessary and sufficient for this nociceptive response, it is more likely that at least some of the tested Innexins play a role in the cold nociception pathway than that knocking down *innexin* expression in Class III da neurons inhibits the larvae's general ability to cringe.

Innexin 1 (Ogre) and Innexin 2 Function Is Required for Cold Nociception While Innexin 8 (ShakingB) Function is Unclear

Since Inx1 (Ogre) is known to function in the central nervous system during the late larval period of *Drosophila* (*45*), I hypothesized that it could be one of the Innexins that functions in the cold nociception pathway of third instar larvae. The Ogre Class III da neuron knockdown group turned out to be the one Class III da neuron knockdown group that showed the greatest raw average percent cringe after knocking it down compared to the other groups (Fig. 15b). This could potentially be interpreted as evidence for Ogre not playing a role in the cold nociception pathway, but the percentage of each Inx RNAi knockdown group of larvae that

classified as non-cringers is the measurement that serves as the proxy for cringe inhibition (Fig. 14). The apparent discord between the maximum average percent cringe values relative to the other knockdown groups and the percentages of non-cringers obtained from comparing the RNAi knockdown groups to their respective non-expression controls demonstrates the need for normalization in order to compare responses across different RNAi constructs. The group of larvae underexpressing Ogre in their Class III da neurons did have a significantly higher percentage of non-cringers (41%) than the non-expressed Ogre RNAi control (5%), supporting the hypothesis that Ogre is involved in the cold nociception pathway (Fig. 14). The role of Ogre in the cold nociceptive pathway will be verified in the future by testing a short hairpin RNA (shRNA) and a viable *ogre* mutant.

Ogre's inability to form homomeric channels in a *Xenopus* expression assay (*46*) suggests it may form heteromeric channels, interacting with another Innexin in the cold nociception pathway. That Innexin could be the one Ogre is known to form channels with, Inx2 (*46*). Consistently, knockdown of Inx2 in Class III da neurons with both RNAi constructs resulted in significantly more non-cringers (32% for construct JF02446 and 76% for construct HMS02481) than the non-expression controls (6% and 4%, respectively), and construct HMS02481 resulted in more non-cringers than even the tetanus toxin control (72%) (Fig. 14). Ogre and Inx2 are required in glial cells for normal postembryonic development of the *Drosophila* central nervous system and they partially colocalize in glial cells and the neuroepithelia (*46*), further suggesting they could form heterotypic channels that mediate the cold nociception pathway.

Besides Inx2, the other Innexin that had significantly more non-cringers when knocked down in Class III da neurons with both RNAi constructs tested against it is Inx4 (Zpg) (Fig. 14). Inx2 and Inx4 are therefore more likely to function in the cold nociception pathway than the

other Innexins. Inx3 was the other Innexin, besides Ogre, that was tested with only one RNAi construct, and this construct also resulted in significantly fewer cringers (Fig. 14). Additional Inx3 RNAi constructs will be tested to verify this result.

I also hypothesized that Inx8 (ShakB) functions in larval cold nociception since it functions in the visually-elicited jump reflex, where it is known to form electrical synapses in the giant fiber system (*36, 37*). Unexpectedly, ShakB is one of the four Innexins that showed conflicting significance between the two RNAi constructs tested (Fig. 14). The ShakB RNAi construct that resulted in a very similar percentage of non-cringers compared to the non-expressed RNAi control was the GD 7794 construct obtained from the Vienna *Drosophila* Resource Center (VDRC). Another RNAi construct obtained from the VDRC was Inx6 GD 3692. Like ShakB[GD7794], Inx6[GD3692] also exhibited a lack of non-cringers, at odds with the other Inx6 RNAi construct tested, JF 02168 (Fig. 14). In describing the construction of the RNAi lines available in the VDRC collection, the authors indicated that some of the RNAi constructs failed to significantly knock down the targeted gene expression (*53*). In these cases, the authors found that co-expression of Dicer-2 enhances knock down expression of the target gene. Therefore, the reason for the inconsistent findings for these genes could be due to differences between the RNAi constructs themselves. The Harvard Group who generated the RNAi constructs obtained from the Bloomington Stock Center (BSC) report the RNAi constructs they constructed do not require enhancement by Dicer-2 (*53, 54*). Consistent with this, the one short hairpin RNA (shRNA) construct obtained from BSC, Inx2 HMS02481, resulted in the greatest cringe inhibition, which is consistent with the idea that shRNAs are more effective at knocking down expression of the target gene than long hairpin RNAs (*44*).To resolve this conflict with the ShakB results, in the future a shRNA construct obtained from BSC will be tested to knock down ShakB expression, and ShakB

mutants will be tested as well. shRNA constructs and mutants will also be tested for the other Innexins, Innexins 5, 6, and 7, whose knockdown resulted in conflicting behavioral outcomes in order to resolve these conflicting results as well.

Tetanus Toxin Expression and Neuronal Synapses

The tetanus toxin (TNTE) line, the control for disrupting Class III da neuron function suggests cells other than Class III da neurons may function in the cold nociception pathway or that chemical synapses are insufficient on their own for transmitting the Class III da neuron signal. Tetanus toxin inhibits neuronal function by cleaving the synaptic vesicle protein synaptobrevin, which results in the loss of neurotransmitter exocytosis (*55*). The fact that tetanus toxin inhibits the cold nociceptive cringe response therefore suggests that release of neurotransmitter, and thus the action of chemical synapses, play a role in the cold nociception pathway. The fact that some cringe response is still seen in the tetanus toxin trial suggests that transmission of the cold nociceptive signals may require synapses in addition to chemical synapses in Class III da neurons. Paired with the evidence that Innexins play a role in the cold nociceptive pathway (Fig. 14), the transmission components that allow a residual cringe response to remain are likely electrical synapses between Class III da neurons. This residual cringe response in the presence of tetanus toxin demonstrates the utility of pairing electrical synapses with chemical ones in vitally important pathways: a high fidelity of signal transmission.

Overall Conclusions

This study suggests electrical synapses function in tandem with chemical ones to transmit cold nociceptive signals via Class III da neurons in *Drosophila melanogaster*. The gap junction proteins most likely to form those electrical synapses are Inx2 and Zpg because those were the Innexins that were knocked down with two different RNAi constructs, which both resulted in significantly more non-cringers than the non-expressed RNAi controls. Ogre and Inx3 also seem to play a role, although the evidence is not as strong, because they were knocked down with only one RNAi construct and these constructs resulted in significantly more non-cringers than the non-expressed RNAi controls.

Future Directions

Lab members are currently working on building *Drosophila* stocks in which a single line possesses both the 19-12 Gal4 driver and either the UAS *ogre* RNAi or UAS *inx2* RNAi responder. This will allow testing of two different *innexin* RNAi knockdowns in individual larvae. This will allow testing of the hypothesis that heteromeric hemichannels function in Class III da neurons. For example, if the hypothesis that Inx2 and Ogre form heteromeric gap junction channels is correct, then the cringe response should be inhibited further than what is seen in the Ogre and Inx2 Class III da neuron knockdowns alone.

In addition to double *innexin* knockdowns in Class III da neurons, the rest of the extant RNAi constructs will be expressed in all da neurons, and the resulting larvae will be tested with the cold behavioral assay. This will allow thorough probing for the involvement of the other classes of da neurons in the cold nociception pathway. The extant viable mutants for *ogre*, *zero*

population growth, and *shakB* will also be tested in the cold behavioral assay. Collectively, these data sets will identify the best Innexins to pursue in future studies.

Besides more extensive reverse genetic screening, molecular analysis will lend more tangible evidence to the hypothesis that Innexins function in the cold nociception pathway. The first step will be to determine which *innexin* genes are expressed as mRNA in wild type Class III da neurons by performing rtPCR and qPCR analysis. Based on the mRNA quantification and cold behavioral assay results, immunohistochemistry will be performed to visualize the location of Innexins that are expressed in Class III da neurons and whose knockdown inhibits the cold-evoked cringe response.

REFERENCES

1. P. Cortelli, G. Giannini, V. Favoni, S. Cevoli, G. Pierangeli, Nociception and autonomic nervous system. *Neurological Sciences.* **34**, 41-46 (2013).

2. C. S. Sherrington, Qualitative difference of spinal reflex corresponding with qualitative difference of cutaneous stimulus. *J. Physiol.* **30**, 39-46 (1903).

3. E. Smith, G. R. Lewin, Nociceptors: a phylogenetic view. *J Comp Physiol A Neuroethol Sens Neural.* **195**, 1089-1106 (2009).

4. N. J. Himmel, D. N. Cox, Sensing the cold: TRP channels in thermal nociception. *Channels.* **11**, 370-372 (2017).

5. M. Baliki, A. Apkarian, Nociception, pain, negative moods and behavior selection. *PubMed Central.* **87**, 474-491 (2016).

6. M. C. Lee, A. Mouraux, G. D. Iannetti, Characterizing the cortical activity through which pain emerges from nociception. *J Neurosci.* **29**, 7909-16 (2009).

7. R. K. Hofbauer, P. Fiset, G. Plourde, S. B. Backman, M. C. Bushnell, Dose-dependent effects of propofol on the central processing of thermal pain. *Anesthesiology.* **100**, 386-94 (2004).

8. L. R. Squire, The Legacy of Patient H.M. for Neuroscience. *Neuron.* **61**, 6-9 (2010).

9. N. Hebben, S. Corkin, H. Eichenbaum, K. Shedlack, Diminished ability to interpret and report internal states after bilateral medial temporal resection: case H.M. *Behav Neurosci.* **99**, 1031-9 (1985).

10. L. Nikolajsen, T. S. Jensen, in Wall & Melzack's Textbook of Pain, McMahon, Stephen, Koltzenburg, Martin, Eds. (Churchill Livingstone, Edinburgh, ed. 5th, 2006), pp. 961-971.

11. R. S. Woodworth, C. S. Sherrington, A pseudaffective reflex and its spinal path. *J Physiol.* **31**, 234-43 (1904).

12. S. Kendroud, A. Hanna, in StatPearls (StatPearls Publishing LLC, Treasure Island, FL, 2018).

13. R. L. Nahin, Estimates of pain prevalence and severity in adults: United States, 2012. *J Pain.* **16**, 769-780 (2015).

14. D. Boudreau *et al.*, Trends in long-term opioid therapy for chronic non-cancer pain. *Pharmacoepidemiol Drug Saf.* **18**, 1166-75 (2009).

15. P. K. Muhuri, J. C. Gfroerer, M. C. Davies, Associations of Nonmedical Pain Reliever Use and Initiation of Heroin Use in the United States. *CBHSQ Data Rev.*(2013).

16. T. J. Cicero, M. S. Ellis, H. L. Surratt, S. P. Kurtz, The Changing Face of Heroin Use in the United States: A Retrospective Analysis of the Past 50 Years. *JAMA Psychiatry.* **71**, 821-826 (2014).

17. R. G. Carlson, R. W. Nahhas, S. S. Martins, R. Daniulaityte, Predictors of transition to heroin use among initially non-opioid dependent illicit pharmaceutical opioid users: A natural history study. *Drug Alcohol Depend.* **160**, 127-134 (2016).

18. US Department of Health and Human Services, CDC, CDC/NCHS, National Vital Statistics System, Mortality. (2018).

19. E. T. Walters, Injury-related behavior and neuronal plasticity: an evolutionary perspective on sensitization, hyperalgesia, and analgesia. *Int. Rev. Neurobiol.* **36**, 325-427 (1994).

20. E. T. Walters, L. L. Moroz, Molluscan memory of injury: evolutionary insights into chronic pain and neurological disorders. *Brain Behav. Evol.* **74**, 206-218 (2009).

21. C. J. Woolf, E. T. Walters, Common patterns of plasticity contributing to nociceptive sensitization in mammals and Aplysia. *Trends Neurosci.* **14**, 74-8 (1991).

22. B. D. Burrell, Comparative biology of pain: What invertebrates can tell us about how nociception works. **117**, 1461-1473 (2017).

23. N. Himmel, A. Patel, D. Cox, Invertebrate Nociception. *Neuroscience.*(2017).

24. H. Turner *et al.*, The TRP Channels Pkd2, NompC, and Trpm Act in Cold-Sensing Neurons to Mediate Unique Aversive Behaviors to Noxious Cold in Drosophila. *Current Biology.*(2016).

25. M. J. Sulkowski, M. S. Kurosawa, D. N. Cox, Growing pains: Development of the larval nocifensive response in Drosophila. *Biol Bull.* **221**, 300-306 (2011).

26. W. B. Grueber *et al.*, Projections of Drosophila multidendritic neurons in the central nervous system: links with peripheral dendrite morphology. *Development.* **134**, 55-64 (2007).

27. R. D'Mello, A. H. Dickenson, Spinal cord mechanisms of pain. *British Journal of Anaesthesia.* **101**, 8-16 (2008).

28. B. Williamson., thesis James Madison University (2015).

29. K. Shimizu, M. Stopfer, Gap junctions. *Current Biology.* **23**, R1031 (2013).

30. R. Bauer *et al.*, Intercellular communication: the Drosophila innexin multiprotein family of gap junction proteins. *Chem Biol.* **12**, 515-26 (2005).

31. E. C. Beyer, V. M. Berthoud, Gap junction gene and protein families: Connexins, innexins, and pannexins. *Biochimica Et Biophysica Acta.* **1860**, 5 (2018).

32. H. Alexopolous *et al.*, Evolution of gap junctions: the missing link? *Current Biology.* **14**, 879 (2004).

33. A. Fein, *Nociceptors and the Perception of Pain* (University of Connecticut Health Center, Farmingto, 2014), pp. 1-6.

34. A. E. Pereda, Electrical synapses and their functional interactions with chemical synapses. *Nat Rev Neurosci.* **15**, 250-263 (2014).

35. Z. Y. Chen *et al.*, Attenuation of Neuropathic Pain by Inhibiting Electrical Synapses in the Anterior Cingulate Cortex. *Anesthesiology.* **124**, 169-83 (2016).

36. P. Phelan *et al.*, Mutations in shaking-B Prevent Electrical Synapse Formation in the Drosophila Giant Fiber System. *The Journal of Neuroscience.* **16**, 1101-1113 (1996).

37. P. Phelan *et al.*, Molecular Mechanism of Rectification at Identified Electrical Synapses in the Drosophila Giant Fiber System. *Current Biology.* **18**, 1955-1960 (2008).

38. J. B. Thomas, R. J. Wyman, Mutations altering synaptic connectivity between identified neurons in Drosophila. *J Neurosci.* **4**, 530-8 (1984).

39. J. M. Blagburn, H. Alexopolous, J. A. Davies, J. P. Bacon, Null mutation in shaking-B eliminates electrical, but not chemical, synapses in the Drosophila giant fiber system: a structural study. *J Comp Neurol.* **404**, 449-58 (1999).

40. A. Fayyazuddin, M. A. Zaheer, P. R. Hiesinger, H. J. Bellen, The nicotinic acetylcholine receptor Dalpha7 is required for an escape behavior in Drosophila. *PLoS Biol.* **4**, e63 (2006).

41. J. B. Duffy, GAL4 System in Drosophila: A Fly Geneticist's Swiss Army Knife. *Genesis.* **34**, 1-15 (2002).

42. D. Lohr, P. Venkov, J. Zlatanova, Transcriptional regulation in the yeast GAL gene family: a complex genetic network. *Faseb J.* **9**, 777-787 (1995).

43. K. Prüßing, A. Voigt, J. B. Schulz, Drosophila melanogaster as a model organism for Alzheimer's disease. *Molecular Neurodegeneration.* **8**, 35 (2013).

44. R. Bartoletti *et al.*, Short hairpin RNA is more effective than long hairpin RNA in eliciting pointed loss-of-function phenotypes in DrosophilaShort hairpin RNA is more effective than long hairpin RNA in eliciting pointed loss-of-function phenotypes in Drosophila. *Genesis.* **55**(2017).

45. H. D. Lipshitz, D. R. Kankel, Specificity of gene action during central nervous system development in Drosophila melanogaster: Analysis of the lethal (1) optic ganglion reduced locus. *Developmental Biology.* **108**, 56-77 (1985).

46. C. E. Holcroft *et al.*, Innexins Ogre and Inx2 are required in glial cells for normal postembryonic development of the Drosophila central nervous system. *Journal of Cell Science.* **126**, 3823-3834 (2013).

47. Y. Xiang *et al.*, Light-avoidance-mediating photoreceptors tile the Drosophila larval body wall. *Nature.* **468**, 921-926 (2010).

48. W. Song, M. Onishi, L. Y. Jan, Y. N. Jan, Peripheral multidendritic sensory neurons are necessary for rhythmic locomotion behavior in Drosophila larvae. *Proc Natl Acad Sci USA.* **104**, 5199-204 (2007).

49. C. A. Schneider, W. S. Rasband, K. W. Eliceiri, NIH Image to ImageJ: 25 years of image analysis. *Nat Methods.* **9**, 671-5 (2012).

50. Y. N. Jan, L. Y. Jan, Branching out: mechanisms of dendritic arborization. *Nature Reviews Neuroscience.* **11**, 449 (2010).

51. W. B. Grueber, L. Y. Jan, Y. N. Jan, Tiling of the Drosophila epidermis by multidendritic sensory neurons. *Development.* **129**, 2867-78 (2002).

52. A. Findsen, T. H. Pedersen, A. G. Petersen, O. B. Nielsen, J. Overgaard, Why do insects enter and recover from chill coma? Low temperature and high extracellular potassium compromise muscle function in Locusta migratoria. *Journal of Experimental Biology.* **217**, 1297-1306 (2014).

53. J. Ni *et al.*, Vector and parameters for targeted transgenic RNA interference in Drosophila melanogaster. *Nat Methods.* **5**, 49-51 (2008).

54. L. A. Perkins *et al.*, The Transgenic RNAi Project at Harvard Medical School: Resources and Validation. *Genetics.* **201**, 843-852 (2015).

55. S. T. Sweeney, K. Broadie, J. Keane, H. Niemann, C. J. O'Kane, Targeted expression of tetanus toxin light chain in Drosophila specifically eliminates synaptic transmission and causes behavioral defects. *Neuron.* **14**, 341-51 (1995).